

Dispersive analysis of the S -, P -, D -, and F -wave $\pi\pi$ amplitudes

P. Bydžovský^a, R. Kamiński^b, V. Nazari^b

^a*Nuclear Physics Institute, Czech Academy of Sciences, Řež, Czech Republic*

^b*Institute of Nuclear Physics, Polish Academy of Sciences, Kraków, Poland*

(Dated: December 4, 2016)

A reanalysis of $\pi\pi$ amplitudes for all important partial-waves below about 2 GeV is presented. A set of once subtracted dispersion relations with imposed crossing symmetry condition is used to modify unitary multi-channel amplitudes in the S , P , D , and F waves. So far, these specific amplitudes constructed in our works and many other analyzes have been fitted only to experimental data and therefore do not fulfill the crossing symmetry condition. In the present analysis, the self consistent, i.e. unitary and fulfilling the crossing symmetry, amplitudes for the S , P , D , and F waves are formed. The proposed very effective and simple method of modification of the $\pi\pi$ amplitudes does not change their previous-original mathematical structure and the method can be easily applied in various other analyzes.

PACS numbers: 11.55.Fv, 11.55.-m, 11.80.Et, 13.75.Lb

Keywords: scalar mesons, dispersion relations, multi-channel amplitudes

I. INTRODUCTION

The enthusiasm in the analysis of $\pi\pi$ interaction amplitudes has been increased significantly quite recently. Especially important were numerous works on dispersive analyzes of experimental data made by Bern [1] and Madrid-Kraków [2] group. The significant progress was made when the analyzes began to effectively use theoretical constraints i.e. crossing symmetry condition imposed on the amplitudes found in experimental analyzes. This was particularly important because of big differences between results obtained by various experimental groups and even between data sets found in the same experimental analysis [3, 4].

Those dispersive analyzes had immediately large impact on the spectroscopy of light scalar mesons (i.e. $f_0(500)$ and $f_0(980)$) which is evident comparing the tables of the Particle Data Group from the years 2010 and 2012 [5, 6]. The analyzes provided also a set of all important amplitudes (S , P , D and F) well describing experimental data up to 1420 MeV and 2000 MeV in case of works done by the Madrid-Kraków and Bern group, respectively. In both those analyzes the S and P wave amplitudes were fitted also to dispersion relations with imposed crossing symmetry constrain below 1100 MeV. The Bern group was using Roy equations [7] which need two subtractions and found analytical solution below 800 MeV. The Madrid-Kraków group also used Roy equations and additionally Roy like ones, so called GKPY equations with only one subtraction what gave more precise output amplitudes. The amplitudes of higher partial-waves, D and F , were also fitted to such dispersion relations but only indirectly by means of the Roy or GKPY equations, i.e. they were present in the kernel part of the equations written for the S and P waves.

An example of practical application of the GKPY equations is our last reanalysis of the S - and P -wave multi-channel amplitudes [8] constructed in a previous

analysis by fitting the experimental data only [9]. One of the most spectacular effects given by the GKPY equations was a shift of the $f_0(500)$ pole by several hundred MeV towards the position indicated by the analyzes of the Bern and Madrid-Kraków group. It is important to note that this reanalysis was done keeping the original mathematical structure of the amplitudes proposed in the work [9].

The aim of this work is to perform similar but more extensive reanalysis of the multi-channel $\pi\pi$ amplitudes including the S , P , D , and F partial waves important in the low energy region (below 2 GeV). The initial amplitudes, in the following denoted as “original”, were fitted only to the experimental data and are taken from our previous analysis ($S0$ [8] and $P1$ [9], hereafter we will use notation ℓI if needed (ℓ -meson-meson partial wave and I -isospin)) or are updated in this work utilizing a form from [10] ($D0$ and $F1$). To perform this analysis we use the GKPY equations for the D and F waves constructed and presented in [11], which have not been used so far in the analysis of amplitudes. The final amplitudes are constrained by both the experimental data and the GKPY dispersion relations (i.e. by crossing symmetry). As the reanalysis is not too much effective for higher partial-waves, particularly for $F1$, parameters of this amplitude are expected to be only weakly changed. In the analysis, only some parameters of the amplitudes are changed which do not alter the mathematical structure of the original amplitudes, similarly as in our previous analysis of the S and P waves [8].

The reanalyzed partial-wave multi-channel amplitudes, constrained also by the crossing symmetry, can be utilized in accounting for the final-state interactions in the decays of heavy mesons and in photoproduction processes, for example, in the CLAS12 and GlueX experiments at JLab. The amplitudes can also be used in constructing a full $\pi\pi$ amplitude giving the cross section at low energies.

The paper is organized as follows: in Section II we

briefly remind the method and results of our previous analysis of the $S0$ and $P1$ partial-wave amplitudes done in [8]. In Section III we present new $D0$ and $F1$ amplitudes fitted to experimental data. In Section IV we detail the method and give results of the dispersive analysis for all considered partial-waves. Section V is devoted to discussion of obtained results. Here we also show results for the low-energy total and differential cross sections in the $\pi^+\pi^-$ scattering. Summary of results is in Section VI.

II. DISPERSIVE ANALYSIS OF THE S - AND P -WAVE AMPLITUDES

In our previous work [8] we reanalyzed the S - and P -wave amplitudes constructed in [9] refitting some of their parameters simultaneously to experimental data and to GKPY dispersion relations. These multi-channel amplitudes are unitary and analytic on the Riemann surface with free parameters that are just positions of poles on different Riemann sheets and few background parameters. Such simple and not biased mathematical structure makes interpretation of obtained results very easy and unambiguous. In analysis [9] these amplitudes were, however, fitted only to very dispersed experimental data from various experiments what resulted in pole positions sometimes very different from those obtained in other analyzes and from those in Particle Data Group Tables.

In the analysis [8] the original mathematical structure of the resonant and background parts of amplitudes from [9] was not changed. The only novelty was a new parameterization of the near threshold amplitudes, which was necessary due to the total lack of description of the phase shifts in this region [9]. Polynomials were, therefore, added to both S and P amplitudes and the phase shifts (values and the first derivatives) were smoothly matched below the $K\bar{K}$ threshold, at about 400 and 600 MeV for the S and P waves, respectively. In Ref. [8] we also constructed a “new” S -wave isoscalar amplitude hereafter called New S -wave fitting its parameters only to the data, what improved behavior of the amplitude. In the subsequent analysis both “Old” [9] and New S -wave isoscalar amplitudes were used.

In analysis [8] the strategy of our work was following: the Old (New) S -wave isoscalar and the old isovector P -wave [9] amplitudes, both supplemented with the near threshold polynomials, were used as the input in the GKPY equations that have a general form

$$\begin{aligned} \text{Re } t_\ell^{I(OUT)}(s) = & \sum_{I'=0}^2 C^{II'} t_0^{I'} (4m_\pi^2) \\ & + \sum_{I'=0}^2 \sum_{\ell'=0}^3 \oint_{4m_\pi^2}^\infty ds' K_{\ell\ell'}^{II'}(s, s') \text{Im } t_{\ell'}^{I'(IN)}(s'), \quad (1) \end{aligned}$$

where $t_{\ell'}^{I'(IN)}(s')$ and $t_\ell^{I(OUT)}(s)$ are the input and output amplitudes, respectively, in a given partial-wave ℓ, ℓ' with

isospin I, I' . The $C^{II'}$ is the crossing matrix constant and $K_{\ell\ell'}^{II'}(s, s')$ are kernels constructed for partial-wave projected amplitudes with the imposed $s \leftrightarrow t$ crossing symmetry condition. The kernels for the S and P waves were presented in [2].

As it is seen in Eq. (1), one has to use the imaginary parts of all important partial-wave amplitudes as an input. We took, therefore, these important amplitudes, $S2, D0, D2$ and $F1$, directly from Ref. [2] and kept them fixed during the analysis. Finally we fitted some parameters of the $S0$ and $P1$ amplitudes simultaneously to the experimental data and to the dispersion relations (1). As a result, the $f_0(500)$ pole moved by several hundred MeV to a new position close to that found in dispersive analyzes [15, 16].

The minimized full χ^2 function was composed of two data terms $\chi_{Data}^2(k)$, related with data in the S and P waves, and of three terms $\chi_{DR}^2(k)$ for the output amplitudes from the dispersion relations

$$\chi^2 = \sum_{k=1}^2 \chi_{Data}^2(k) + \sum_{k=1}^3 \chi_{DR}^2(k), \quad (2)$$

where $k = 1, 2, 3$ itemizes, respectively ℓI partial-waves: the $S0, P1$ and $S2$. Corresponding $\chi_{Data}^2(k)$ and $\chi_{DR}^2(k)$ were expressed by

$$\chi_{Data}^2(k) = \sum_{i=1}^{N_\delta^k} \frac{(\delta_i^{exp} - \delta_i^{th})^2}{(\Delta\delta_i^{exp})^2} + \sum_{i=1}^{N_\eta^k} \frac{(\eta_i^{exp} - \eta_i^{th})^2}{(\Delta\eta_i^{exp})^2} \quad (3)$$

and

$$\chi_{DR}^2(k) = \sum_{i=1}^{N_{DR}} \frac{\left[\text{Re } t_\ell^{I(OUT)}(s_i) - \text{Re } t_\ell^{I(IN)}(s_i) \right]^2}{\left[\Delta \text{Re } t_\ell^{I(OUT)}(s_i) \right]^2}, \quad (4)$$

where δ_i^{exp} (or η_i^{exp}) and δ_i^{th} (or η_i^{th}) are experimental and our-theoretical phase shifts (or inelasticities) and N_δ^k (or N_η^k) are numbers of the data points for phase shifts (or inelasticities) of the $S0$ and $P1$ partial-waves in considered coupled channels. Symbol N_{DR} is a number of energy points between the $\pi\pi$ threshold and 1100 MeV, at which we calculated $\chi_{DR}^2(k)$ (for all three waves $N_{DR} = 26$ was chosen) and $\Delta \text{Re } t_\ell^{I(OUT)}(s_i)$ are fixed to 0.01 in order to make the $\chi_{DR}^2(k)$ comparable with the $\chi_{Data}^2(k)$.

Let us here notice that terms $\chi_{DR}^2(k)$ are in fact not χ^2 functions but rather squared weighted differences between the input and output amplitudes. For simplicity we keep, however, the name χ^2 for these terms.

III. NEW ANALYSIS OF THE D - AND F -WAVE EXPERIMENTAL DATA

The experimental data for the $\pi\pi$ scattering in the $D0$ and $F1$ waves were analyzed in Refs. [9, 10] to study the f_2 and ρ_3 mesons. In presented here analysis the

S-matrix formalism for N coupled channels was utilized similarly as in our previous dispersive analysis of S and P waves [8]. Due to the large number of opened channels in the D and F waves the uniformizing variable (see Eq. (1) in [8]) could not be used and therefore, the Jost matrix determinant was constructed using the multi-channel Breit-Wigner forms.

In the present analysis we have used the same formalism for the $D0$ and $F1$ waves as in Refs. [9, 10] and updated the list of contributing resonance states for the $D0$ wave according to the latest issue of PDG [14]. The corresponding free parameters were fitted to experimental data. In the case of $F1$ wave we have found that enough is only one resonance state $\rho_3(1690)$ and have constructed a reasonable description also in the threshold region. These updated $D0$ and $F1$ amplitudes were then used in the analysis with the GKPY equations taken from [11] (see IV C). In the following subsections we give more details on the formalism and construction of the New $D0$ and New $F1$ amplitudes.

A. Formalism

The matrix elements S_{ij} of the N -channel S matrix ($i, j = 1, 2, \dots, N$) are expressed via the Jost matrix determinant, $d(k_1, k_2, \dots, k_N)$ (k_i are the channel momenta), using the Le Couteur–Newton relations [9, 10]. These expressions together with the formulas of analytical continuation of the matrix elements to the unphysical sheets naturally generate the resonance poles and zeros on the Riemann surface. The Jost determinant is considered in a separable form $d = d_{bgr} d_{res}$. The resonance part is described by the multi-channel Breit-Wigner form

$$d_{res} = \prod_r \left[M_r^2 - s - i \sum_{j=1}^N \rho_{rj}^{2J+1} R_{rj} f_{rj}^2 \theta(s - s_j) \right], \quad (5)$$

where s is the invariant total energy squared, M_r and $J = \ell$ are the resonance mass and spin, respectively, $\rho_{rj} = 2k_j / \sqrt{M_r^2 - s_j}$ with s_j the channel thresholds, R_{rj} are the Blatt-Weisskopf barrier factors, and the free parameter f_{rj} is related with a decay width of a resonance r into a channel j .

The background part d_{bgr} , which represents mainly an influence of neglected channels and resonances, adds in general an energy dependent phase in each channel.

B. Fits for the D wave

In the analysis of the data in the tensor-isoscalar sector we have considered explicitly the channels: 1- $\pi\pi$, 2-effective $(2\pi)(2\pi)$, 3- $K\bar{K}$, and 4- $\eta\eta$. The resonant part of the Jost determinant, $d(k_1, k_2, k_3, k_4)$, is then given by the four-channel Breit-Wigner form (5) with $J = 2$ and

the barrier factor

$$R_{rj} = \frac{9 + \frac{3}{4}(\sqrt{M_r^2 - s_j} r_{rj})^2 + \frac{1}{16}(\sqrt{M_r^2 - s_j} r_{rj})^4}{9 + \frac{3}{4}(\sqrt{s - s_j} r_{rj})^2 + \frac{1}{16}(\sqrt{s - s_j} r_{rj})^4}, \quad (6)$$

where the radii r_{rj} have a common value 0.943 fm [10] which was kept constant in our analysis.

In the set of resonance states contributing to the process we have considered eleven states presented in the PDG summary table [14]: $f_2(1270)$, $f_2(1430)$, $f_2(1525)$, $f_2(1640)$, $f_2(1810)$, $f_2(1910)$, $f_2(1950)$, $f_2(2010)$, $f_2(2150)$, $f_2(2300)$, $f_2(2340)$. We have not included the broad state $f_2(1565)$ which was not listed in the previous issue of PDG and which can be mimic by the nearby state $f_2(1525)$. The masses of the resonances were taken from the PDG tables but in the course of fitting $f_2(1430)$, $f_2(1525)$, $f_2(2010)$, $f_2(2300)$ and $f_2(2340)$ resonance masses were allowed to change slightly within an interval of several standard deviations around the central value. The partial widths of the resonances, the parameters f_{rj} in (5), were fitted to the data.

The background part of the Jost determinant was taken from [9] and has the form

$$d_{bgr} = \exp \left[-i \sum_{j=1}^4 \left(\frac{2k_j}{\sqrt{s}} \right)^5 (a_j + ib_j) \right], \quad (7)$$

where $a_2 = a_3 = a_4 = 0$,

$$a_1 = \alpha_{11} + \frac{s - s_3}{s} \alpha_{13} \theta(s - s_3) + \frac{s - s_v}{s} \alpha_{10} \theta(s - s_v),$$

$$b_j = \beta_j + \frac{s - s_v}{s} \gamma_j \theta(s - s_v), \quad \text{for } j = 1, 3, 4,$$

and $b_2 = 0$. The threshold $s_v = 2.274 \text{ GeV}^2$ accounts for effects from the channels $\eta\eta'$, $\rho\rho$, and $\omega\omega$ not included explicitly in the analysis. The parameters α_{11} , α_{13} , α_{10} , β_j , and γ_j were fitted to the data.

The experimental data for the $\pi\pi$ scattering are from the energy-independent analysis by Hyams et al. [12] and the data for inelastic scattering $\pi\pi \rightarrow K\bar{K}, \eta\eta$ from Ref. [13]. To warrant a right behavior of the elastic phase shifts in the threshold region, i.e. a consistency with the scattering length and the slope parameter taken from [2], we have included in the data set also the sixteen points (pseudo data) generated in the range 282-825 MeV by the phenomenological amplitudes [2] with errors about 10%.

In successive fitting of the parameters to the data we found a solution with $\chi^2/n.d.f. = 242.28/(199 - 58) = 1.72$ where the value without the pseudo data is $\chi^2/n.d.f. = 239.28/(183 - 58) = 1.91$. The parameters of resonances of the New $D0$ amplitude are given in Table I and a comparison with the old $D0$ amplitude [9] is shown in Figs. 1 and 2. The background parameters are: $\alpha_{11} = 0.00096$, $\alpha_{13} = -0.04105$, $\alpha_{10} = -0.186$, $\beta_1 = -0.0531$, $\beta_3 = -1.99$, $\beta_4 = -1.47$, $\gamma_1 = 0.00128$, $\gamma_3 = 1.99$, and $\gamma_4 = 1.43$.

state	PDG	M_r	f_{r1}	f_{r2}	f_{r3}	f_{r4}
$f_2(1270)$	1275.5 ± 0.8	1275.5	459.3	0.001	204.0	91.3
$f_2(1430)$	1430	1463.2	42.3	0.12	346.8	0.02
$f_2(1525)$	1525 ± 5	1570.7	0.01	207.5	128.4	96.3
$f_2(1640)$	1639 ± 6	1639.0	145.3	524.4	430.5	233.5
$f_2(1810)$	1815 ± 12	1815.0	163.5	279.2	497.2	590.3
$f_2(1910)$	1903 ± 9	1903.0	0.077	65.3	0.067	371.3
$f_2(1950)$	1944 ± 12	1944.0	5.01	59.5	625.7	97.9
$f_2(2010)$	2011 ± 62	2027.0	0.001	146.4	457.1	0.5
$f_2(2150)$	2157 ± 12	2157.0	0.015	445.8	148.1	354.6
$f_2(2300)$	2297 ± 28	2181.6	78.14	74.9	818.3	169.5
$f_2(2340)$	2345 ± 40	2383.3	46.20	7.1	633.2	163.8

TABLE I: Parameters of the Breit-Wigner form (in MeV) for the New $D0$ amplitude. The masses of the resonances from PDG [14] are also shown in the second column.

This solution is a bit worse (the χ^2) than that in Ref. [9] (χ^2 was $156.62/(168 - 69) = 1.58$) but we have achieved the right behavior of δ_{11} for energies below 800 MeV (see the detail in Fig. 1(a)) which allows us to avoid a polynomial-like extension of the phase shift as in the case of the S and P amplitudes. In Figs. 1 and 2 for inelasticity η_{11} and the squared modulus of the S matrix in inelastic channels one can see even a slight improvement in description of the data. Please notice also that the set of resonances and their masses are in a good agreement with the PDG tables, see Table I.

C. Fits for the F wave

In the isovector F wave, there are only two resonance states listed in the PDG summary table which are relevant for the data description below 2 GeV: $\rho_3(1690)$ and $\rho_3(1990)$ [14]. For the former, the decay widths into the $\pi\pi$, $\pi^\pm\pi^+\pi^-\pi^0$, $\omega\pi$, $K\bar{K}$ and $K\bar{K}\pi$ channels are well established whereas for the latter the partial widths are not known. To learn on importance of these resonances in description of data we performed fits in [17] (Tables V and VI). We showed that if both resonances are fitted simultaneously then the mass of $\rho_3(1990)$ turns into a huge number showing that one resonance state is enough to achieve a reasonable data description. We have therefore considered only $\rho_3(1690)$ in the analysis of the phase shift and inelasticity parameter in the $\pi\pi$ scattering [12]. This state is also apparently well seen in the pronounced data structure.

In the analysis we have included four channels: 1- $\pi\pi$, 2- effective $(2\pi)(2\pi)$, 3- $\omega\pi$, and 4- $K\bar{K}$. The Blatt-Weisskopf barrier factor in the Breit-Wigner form (5) was in the case of $J = 3$

$$R_{1j} = \frac{225 + 45(\mu_j r_{1j})^2 + 6(\mu_j r_{1j})^4 + (\mu_j r_{1j})^6}{225 + 45(2k_j r_{1j})^2 + 6(2k_j r_{1j})^4 + (2k_j r_{1j})^6}, \quad (8)$$

where μ_j is equal to $\sqrt{M_1^2 - s_j}$. The radii r_{1j} possess a

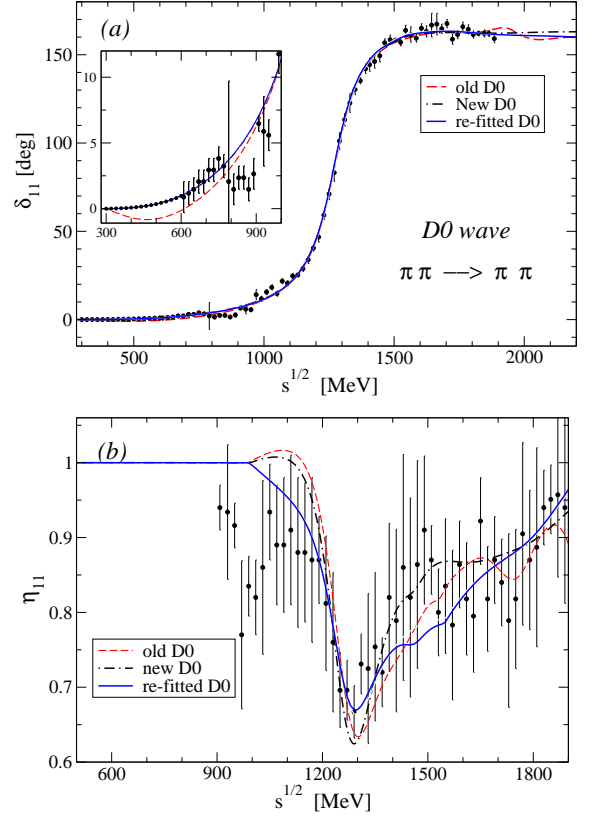


FIG. 1: Results of the New $D0$ (dashed-dotted line), old $D0$ [9] (dashed line) and re-fitted (after fitting to data and dispersion relations) $D0$ (solid line) amplitudes for the phase shift (a) and inelasticity (b) of the $\pi\pi \rightarrow \pi\pi$ scattering are compared with experimental data from Ref. [12] and the pseudo data.

common value 0.927 fm [10] that were kept constant in our analysis. The resonance mass and the Breit-Wigner parameters f_{1j} were fitted to the data.

In our analysis the dispersion relations directly affect only the energy region below 1100 MeV but the higher energy region, where the $\rho_3(1690)$ resonance is clearly seen, is influenced indirectly. The $F1$ amplitude is, therefore, almost entirely determined by the experimental data. Since the resonance state is described by the Breit-Wigner form, which works well only in a vicinity of the resonance, we had to take a particular care of behavior of the amplitude below about 1000 MeV. We have, therefore, chosen a simple modification of the phase shift by means of the background phase in the form of the quadratic polynomial of s

$$d_{bgr} = \exp \left[-i \left(\frac{2k_1}{\sqrt{s}} \right)^7 \left(a_\alpha + \frac{4k_1^2}{s_1} a_\beta + \left(\frac{4k_1^2}{s_1} \right)^2 a_\gamma \right) \right], \quad (9)$$

where k_1 is equal to $\sqrt{s - s_1}/2$ and the parameters a_α , a_β , and a_γ were fitted to the data. Similarly as in the case of the $D0$ wave we have included pseudo data points but now 31 for energies $282 \text{ MeV} < \sqrt{s} < 895 \text{ MeV}$. These

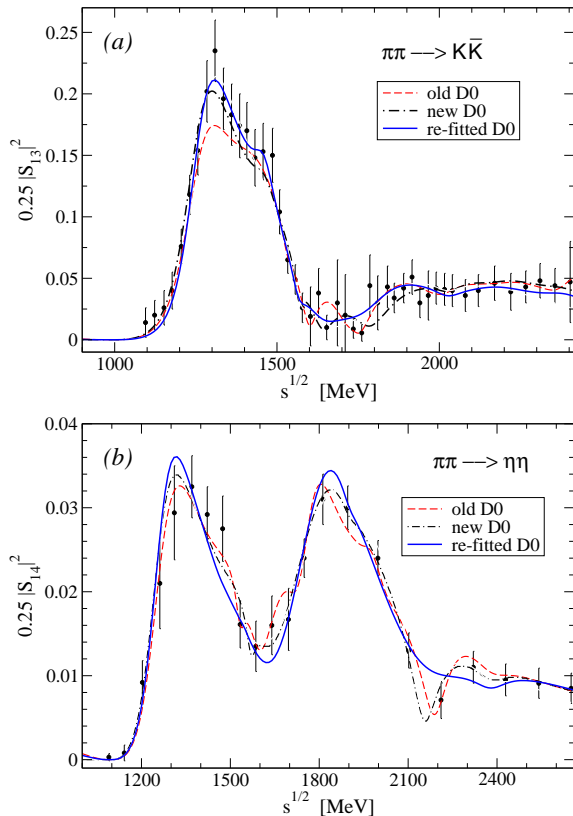


FIG. 2: The same as in Fig. 1 for the squared modulus of the S matrix for the $\pi\pi \rightarrow K\bar{K}$ (a) and $\pi\pi \rightarrow \eta\eta$ (b).

data were generated by the phenomenological parameterization of the amplitudes [2], which ensure the right values of the scattering length and slope parameter given in [2].

In the fitting with the four-channel form we found that only the channels 1 and 2 are important whereas the parameters f_{13} and f_{14} were almost zero. This corresponds quite well with the observed decay rates of the $\rho_3(1690)$ resonance: $23.6 \pm 1.3\%$, $67 \pm 22\%$, $16 \pm 6\%$, $3.8 \pm 1.2\%$, and $1.58 \pm 0.26\%$ into the $\pi\pi$, $\pi^\pm\pi^+\pi^-\pi^0$, $\omega\pi$, $K\bar{K}\pi$, and $K\bar{K}$ channels, respectively [14]. We did therefore a two-channel fit with $\chi^2/n.d.f. = 136.20/(108 - 6) = 1.34$ where the value without the pseudo data is $\chi^2/n.d.f. = 80.84/(77 - 6) = 1.38$ showing that the pseudo data are quite consistent with the experimental data used in the analysis. The resonance parameters are shown in Table II and the background parameters are $a_\alpha = 0.000008$, $a_\beta = -0.000998$, and $a_\gamma = 0.000016$. These parameters are quite small but they play an important role. In the fit with only the first term in (9) the $\chi^2/n.d.f. = 4.0$ where the main contribution comes from the pseudo data. This we consider as a strong evidence of the need for the nonzero additional terms in (9).

To verify that the experimental data can be described purely by one state $\rho_3(1690)$ we fitted only the data with one Breit-Wigner form without background and assum-

state	PDG	M_r	f_{r1}	f_{r2}	f_{r3}	f_{r4}
$\rho_3(1690)$	1688.8 ± 2.1	1714.0	293.1	498.3	0.0	0.0

TABLE II: Parameters of the Breit-Wigner form (in MeV) for the New $F1$ amplitude. The mass of the resonance from PDG [14] is shown in the second column.

ing two channels 1 and 2 (so called “d-fit”). The free parameters acquired similar values as those in the previous fit (Table II): $M_r = 1715.9$, $f_{11} = 294.0$, and $f_{12} = 498.7$. The quality of the fit is a bit worse than of the previous one, $\chi^2/n.d.f. = 110.18/(77 - 3) = 1.49$ (compare the value of $\chi^2/n.d.f.$ without the pseudo data), but this fit clearly demonstrates that the resonance patterns revealed by both the phase shift and the inelasticity parameter are produced by single state $\rho_3(1690)$. The fit, however, overpredicts the pseudo data on δ_{11} in the threshold energy region (see the detail in Fig. 3(a)) and the calculated scattering length is by a factor 2 larger than the value obtained from the GKPY equation [2].

Results of the New $F1$ amplitude and of the simple fit only to the experimental data without background are compared with the data and with the old $F1$ amplitude [10] in Fig. 3. The result of d-fit for δ_{11} is shifted upward with respect to the New $F1$ in the whole considered energy region. These results confirm necessity to introduce the background part of the amplitude (9) to describe correctly the pseudo data. Improvement is apparent also for energies above 1.8 GeV. The resonance pattern seen in Fig. 3(b) is a little bit narrower for the New $F1$ amplitude than for the old one.

IV. RESULTS OF THE DISPERSIVE ANALYSIS FOR THE S -, P -, D -, AND F -WAVE $\pi\pi$ AMPLITUDES

A. Method of analysis

The method of analysis is generally the same as in our previous work [8] which was briefly recalled in the Section II. As the initial amplitudes in the dispersive analysis we used the New $S0$ -wave amplitude from [8] and the Old $P1$ amplitude from [9], both with added polynomial near the threshold (the “extended” amplitudes in Ref. [8]). For the $D0$ and $F1$ waves we used the New amplitudes constructed in Sect. III and a correct behavior of the phase shift near the threshold was controlled by the pseudo data as in Sect. III. Since there are no resonances for $S2$ and $D2$ waves, the amplitudes for these isotensor waves were taken from [2] and kept unchanged during the analysis. The analysis was performed with the same GKPY equations for the S and P waves as in Ref. [8] and with the GKPY equations for the D and F waves from the work [11]. In the modification of the amplitudes we allowed to change only those parameters that were expected to contribute significantly to the dispersive

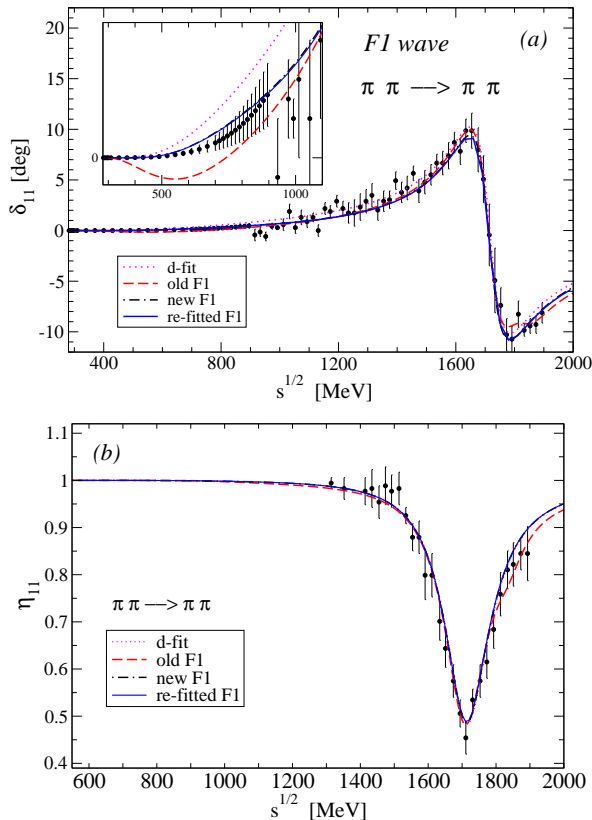


FIG. 3: Results of the New $F1$ (dash-dotted line), old $F1$ [10] (dashed line), the fit only to the experimental data (dotted line) and refitted (after fitting to data and dispersion relations) $F1$ (solid line) amplitudes for the phase shift (a) and inelasticity parameter (b) of the $\pi\pi \rightarrow \pi\pi$ scattering are compared with experimental data from Ref. [12] and the pseudo data (see the detail in (a)).

integrals, i.e. the low-energy resonances and the $\pi\pi$ background. Definitions of the χ^2 functions were analogous to Eqs. (2-4).

The analysis was split into three steps. In the first step, (*the SP analysis*), only the $S0$ and $P1$ amplitudes were modified. In the fitting procedure, the matching energy and parameters of only $f_0(500)$ and $f_0(980)$ resonances and of the $\pi\pi$ background were free in the $S0$ wave. Likewise in the $P1$ wave the matching energy and parameters of background and only the $\rho(770)$ resonance were fitted. Note that contrary to Ref. [8] the parameters of $f_0(1500)$ were not changed. Therefore the number of free parameters in the SP analysis decreased to 31. To make a comparison with the results from [8] possible we used in this step the phenomenological $D0$ and $F1$ amplitudes [2] as in [8].

In the second step, (*the DF analysis*), we used the final $S0$ and $P1$ amplitudes from the SP analysis and the New $D0$ and $F1$ from Sect. III as initial amplitudes. In this step, only the latter two amplitudes were successively modified fitting the parameters of the Breit-Wigner forms of the $f_2(1270)$, $f_2(1525)$, $f_2(1640)$, $f_2(1810)$, $f_2(2125)$,

and $f_2(2300)$ and $\rho_3(1690)$ resonances for the $D0$ and $F1$ partial-waves, respectively, together with the background parameters. The number of free parameters in the DF analysis was 31.

In the third step, (*the SPDF analysis*), we started with the $S0$ and $P1$ amplitudes from the SP analysis and with the $D0$ and $F1$ amplitudes from the DF analysis. In this step we fitted again all free parameters considered above and arrived at the final form of all four amplitudes that we denote “re-fitted”. These amplitudes are optimized to the data and are consistent with the GKPY equations.

B. Results of the SP analysis

Values of the χ^2 for each contribution in the SP analysis are presented distinctly in Tables III and IV. The total $\chi^2/n.d.f.$ is $622.36/(572 - 31) = 1.15$ which is the same value as that obtained in Ref. [8] despite the fact that here we did not include the $f_0(1500)$ state. This justifies omitting parameters of $f_0(1500)$ from the set of free parameters and confirms a stability of the results. Comparing the $\chi^2/n.d.f.$ with the initial one ($\chi^2/n.d.f. = 1520.3/541 = 2.81$) shows a big improvement in the fitting.

The components of the χ^2_{Data} in the $S0$ wave have generally improved with a substantial change in the $\pi\pi \rightarrow \pi\pi$ and $K\bar{K}$ channels. Although the result in the $\pi\pi \rightarrow \eta\eta'$ channel is worse, the total χ^2_{Data} improves noticeably as in Ref. [8]. For the $P1$ wave, χ^2_{Data} of the δ_{11} slightly improves but it is slightly worse for η_{11} . As it was expected a substantial improvement was in the χ^2 of the dispersion relations for $S0$ like in Ref. [8] which is due to the crossing symmetry. The 50% improvement in the χ^2_{DR} for $P1$ is produced mainly by changes in the $S0$ wave which is coupled to $P1$ via the kernel in the GKPY equations (1).

S0 wave						
	χ^2_{Data}	δ_{11}	η_{11}	δ_{12}	$ S_{12} $	$ S_{13} $
initial	321.8	132.9	23.0	126.4	35.6	3.89
re-fitted-SP	282.9	118.8	19.4	118.1	21.3	5.40
P1 wave						
	χ^2_{Data}	δ_{11}	η_{11}			
initial	302.8	264.1	38.7			
re-fitted-SP	301.7	262.4	39.3			

TABLE III: Values of χ^2 for data in the $S0$ and $P1$ waves before (initial) and after (re-fitted-SP) fitting in the SP analysis.

C. Results of the DF analysis

In order to improve agreement of the $D0$ and $F1$ wave amplitudes constructed in sections IIIB and IIIC with

	χ^2_{DR}	$S0$	$S2$	$P1$
initial	895.7	842.9	8.43	44.3
re-fitted-SP	37.8	7.32	10.3	20.2

TABLE IV: Values of χ^2 for the dispersion relations for the $S0$ and $P1$ waves before (initial) and after (re-fitted-SP) fitting in the SP analysis.

crossing symmetry condition, the New $D0$ and New $F1$ amplitudes have been fitted to the GKP dispersion relations and to the data, where the $S0$ - and $P1$ -wave amplitudes were from the SP analysis (section IV B) and remained fixed. Hence, the total χ^2 in Eq. (2) was composed of eight parts: two parts for $\chi^2_{Data}(k)$ in Eq. (3) for $D0$ and $F1$ partial-waves and six parts for $\chi^2_{DR}(k)$ in Eq. (4) for all partial-waves, namely $S0$, $S2$, $P1$, $D0$, $D2$ and $F1$.

D. Results of the SPDF analysis

In the third-last step of our analysis, the total χ^2 in Eq. (2) was composed of ten parts. Four parts for $\chi^2_{Data}(k)$ in Eq. (3) for $S0$, $P1$, $D0$, and $F1$ partial-waves and six parts for $\chi^2_{DR}(k)$ in Eq. (4) for all considered partial-waves, namely $S0$, $S2$, $P1$, $D0$, $D2$, and $F1$.

$S0$ wave						
	χ^2_{Data}	δ_{11}	η_{11}	δ_{12}	$ S_{12} $	$ S_{13} $
initial	321.8	132.9	23.0	126.4	35.6	3.89
re-fitted	292.2	129.3	19.2	117.5	21.1	5.02

$P1$ wave			
	χ^2_{Data}	δ_{11}	η_{11}
initial	302.8	264.1	38.7
re-fitted	299.3	260.7	38.6

TABLE V: Values of χ^2 for data in the $S0$ and $P1$ waves before (initial) and after (re-fitted) fitting in the SPDF analysis.

$D0$ wave						$F1$ wave		
	χ^2_{Data}	δ_{11}	η_{11}	$ S_{13} $	$ S_{14} $	χ^2_{Data}	δ_{11}	η_{11}
initial	242.3	137.0	76.7	21.1	7.44	136.5	120.4	16.1
re-fitted	218.7	128.3	64.1	18.1	8.1	137.3	120.8	16.6

TABLE VI: Values of χ^2 for data in the $D0$ and $F1$ waves before (initial) and after (re-fitted) fitting in the SPDF analysis.

The value of the χ^2 in the SPDF analysis after fitting to the data and dispersion relations is $\chi^2/n.d.f. = 1061.5/895 = 1.19$ which is almost the same as the value in the SP analysis though it includes also contributions of χ^2_{Data} from the multi-channel $D0$ and $F1$ amplitudes.

	χ^2_{DR}	$S0$	$S2$	$P1$	$D0$	$D2$	$F1$
initial	313.2	107.8	24.4	18.0	125.1	16.8	21.2
re-fitted	113.9	5.05	17.9	27.8	27.5	15.8	19.9

TABLE VII: Values of χ^2 for the dispersion relations for all waves before (initial) and after (re-fitted) fitting in the SPDF analysis.

Remind that in the SP analysis we used phenomenological parameterizations of the $D0$ - and $F1$ -wave $\pi\pi$ amplitudes from [2].

Tables V-VII show the χ^2 of the data and the dispersion relations for all waves distinctly. The values of the χ^2_{Data} for the $S0$ and $D0$ waves have generally improved except in the $\pi\pi \rightarrow \eta\eta'$ channel for the $S0$ wave and $\pi\pi \rightarrow \eta\eta$ channel for the $D0$ one. Description of data in this inelastic channel tends to be worse for both $S0$ and $D0$ waves (see $|S_{13}|$ in Table V and $|S_{14}|$ in Table VI) which can be attributed to the coupling between these two waves. Description of data in the $P1$ wave slightly improved for both phase shift and inelasticity. The χ^2_{Data} for the $F1$ wave almost did not change because the parameters of the New $F1$ amplitude are not too much affected by fitting the dispersion relations. All components of the χ^2_{DR} , except that for $P1$, are smaller after fitting with a substantial improvement for the $S0$ and $D0$ waves.

Note that the initial values of the χ^2_{DR} for the $S0$ and $P1$ waves in Table VII differ from the final values in Table IV due to different $D0$ and $F1$ amplitudes used in the analysis. In the SP analysis, the $D0$ and $F1$ amplitudes are from [2] and not modified while in the SPDF analysis we used the New $D0$ and New $F1$ amplitudes. It is especially well seen for the initial value of the χ^2_{DR} for the $P1$ wave which is smaller in the SPDF analysis (18.0) than in the SP one (44.3). Finally it becomes larger but still comparable with the final value in the SP analysis. This suggests quite strong influence of the other amplitudes (especially New $F1$) on the $P1$ amplitude in the dispersive analysis.

Comparing results of the SPDF and SP analysis for the $S0$ wave we see that description of the phase shift δ_{11} is slightly worse in the SPDF analysis. This we attribute to the influence of the New $D0$ and New $F1$ amplitudes, especially of the former as there is stronger correlation between these two waves ($S0$ and $D0$). This can be particularly well seen in a comparison of the final (re-fitted-SP) values of χ^2_{DR} for $S0$ and $S2$ in Table IV with the initial values in Table VII.

In Table VIII we show influence of fitting parameters of the $f_0(1500)$ on the results in the SP and SPDF analyses to see significance of this resonance in the analysis. As it was expected from the previous analysis in Ref. [8] for the S and P waves, results are not too much sensitive to changes of the $f_0(1500)$ -resonance parameters. Although the χ^2 is smaller when parameters of $f_0(1500)$ resonance are free, the $\chi^2/n.d.f.$ do not change. This corroborates our previous results of the analysis in Ref. [8] where pa-

rameters of $f_0(1500)$ changed very slightly.

	$\chi^2/n.d.f.$ ($f_0(1500)$ fixed)	$\chi^2/n.d.f.$ ($f_0(1500)$ free)
$\chi^2(\text{SP})$	622.4/541=1.15	609.7/529=1.15
$\chi^2(\text{SPDF})$	1061.5/895=1.19	1053.6/883=1.19

TABLE VIII: Values of the $\chi^2/n.d.f.$ for the SP and SPDF analyzes when parameters of the $f_0(1500)$ resonance are fixed or free in fitting.

V. DISCUSSION

In Tables IX - XII, we provide a comparison of parameters of the original (“New” amplitude from [8] in case of the $S0$ wave) and re-fitted $S0$ - and $P1$ -wave amplitudes in the SPDF analysis. A substantial change of the parameters after the analysis is a shift of the position of the σ pole on sheet II. The new pole position, $(477.6 \pm 14 - i302.0 \pm 14 \text{ MeV})$ is within three standard deviations consistent with the result in Ref. [8], $(445.2 \pm 14 - i296.4 \pm 14 \text{ MeV})$ demonstrating a stability of the results. This new value is also compatible with that presented by Particle Data Group [14] $(400 - 550) - i(200 - 350) \text{ MeV}$. The pole positions of the $f_0(980)$ resonance did not change too much. The real and imaginary parts became only slightly smaller and are compatible with the values presented in [8]. In the $P1$ wave, the position of the $\rho(770)$ -pole on the Riemann sheet VI was shifted significantly toward smaller energies and closer to the real axis. This, however, does not affect a data description as this pole is far from the physical region. Note, however, that the sheet VI is directly connected with the physical one above the $\rho\sigma$ threshold and therefore a pole lying on the sheet VI near the real axis above the $\rho\sigma$ threshold, in many cases, can influence appreciably description of the data.

The background parameters of the $S0$ and $P1$ waves changed moderately showing that the background part plays only a marginal role in the amplitude. The matching energy $\sqrt{s_{00}}$ became bigger in comparison to that in [8]. One may attribute this to the influence of the New $D0$ wave. On the contrary the matching energy $\sqrt{s_{01}}$ for the $P1$ wave is similar to that in [8]. For the $P1$ wave the background parameter b acquired a very small negative value which affects inelasticity of the $P1$ wave, slightly violating unitarity for energies near 1.8 GeV (see Fig. 6(b)).

Figures 4 - 6 illustrate the results of the re-fitted $S0$ and $P1$ amplitudes for the phase shift and inelasticities in the $\pi\pi \rightarrow \pi\pi$, $K\bar{K}$ and $\eta\eta'$ channels compared to the original amplitudes and available experimental data. Our final results describe the data very well in all considered channels. An improvement is especially apparent for the elastic phases δ_{11} for both waves in the low-energy region. The turn observed at 1.28 GeV in Fig. 4(b) for inelasticity

Sheet		original	re-fitted
$f_0(500)$			
II	E_r	562.9	477.6
	$\Gamma_r/2$	417.1	302.0
III	E_r	594.7	717.6
	$\Gamma_r/2$	417.1	300.4
VI	E_r	615.1	422.2
	$\Gamma_r/2$	417.1	448.5
VII	E_r	583.3	602.7
	$\Gamma_r/2$	417.1	206.7
$f_0(980)$			
II	E_r	1007.6	999.6
	$\Gamma_r/2$	29.4	21.0
III	E_r	984.5	975.5
	$\Gamma_r/2$	55.1	22.1

TABLE IX: Real (E_r) and imaginary ($\Gamma_r/2$) parts of poles on the Riemann sheets of two lowest resonances in the $S0$ amplitude before (original) and after (re-fitted) the full analysis. The values are in MeV.

Parameter	original	re-fitted
a_{11}	-0.0131	-0.07870
$a_{1\sigma}$	0.0	0.13210
$a_{1\nu}$	0.046	-0.13380
$a_{1\eta}$	-0.0302	-0.01832
$b_{1\sigma}$	0.0	0.09207
$b_{1\nu}$	0.0573	0.01855
$b_{1\eta}$	0.0	-0.03753
$\sqrt{s_{00}}$	406.5	495.0

TABLE X: Values of the background parameters and the matching energy $\sqrt{s_{00}}$ (in MeV) for the $S0$ wave before (original) and after (re-fitted) the full analysis.

of the $S0$ wave in $\pi\pi \rightarrow \pi\pi$ is due to opening of the $\sigma\sigma$ channel included in the background part [8].

The new (re-fitted) parameters of the $D0$ and $F1$ waves in the SPDF analysis are given in Tables XIII and XIV. The re-fitted background parameters of the $D0$ amplitude are: $\alpha_{11} = 0.0011853$, $\alpha_{13} = 0.037747$, $\alpha_{10} = -0.46722$, $\beta_1 = 0.15631$, $\beta_3 = -8.5280$, $\beta_4 = -11.4446$, $\gamma_1 = -0.31272$, $\gamma_3 = 9.9804$, and $\gamma_4 = 14.8899$. The re-fitted background parameters of the $F1$ amplitude are: $a_\alpha = 0.0000132$, $a_\beta = -0.00102$, and $a_\gamma = 0.0000151$. Note that contributions of the big magnitudes of the parameters β_3 and γ_3 in the $K\bar{K}$ channel and β_4 and γ_4 in the $\eta\eta$ channel tend to cancel each other above the effective vector-vector channel (s_v) in the background part, see the formulas and text below Eq. (7). Similar correlations between β_j and γ_j were observed also in the data analysis performed in Sect. IIIB.

A comparison of Tables II and XIV shows that the parameters of the $F1$ wave changed only slightly as it

Sheet		original	re-fitted
$\rho(770)$			
II	E_r	766.0	765.4
	$\Gamma_r/2$	72.5	73.0
III	E_r	758.7	799.4
	$\Gamma_r/2$	72.5	53.7
VI	E_r	753.5	1.28
	$\Gamma_r/2$	72.5	0.49
VII	E_r	760.8.2	1051.5
	$\Gamma_r/2$	72.5	8.09

TABLE XI: The same as in Table IX but for the $\rho(770)$ resonance in the $P1$ wave.

Parameter	original	re-fitted
a	-0.2860	-0.33148
b	0.00012	-0.00008
$\sqrt{s_{01}}$	643.6	637.3

TABLE XII: The same as in Table X but for the $P1$ wave.

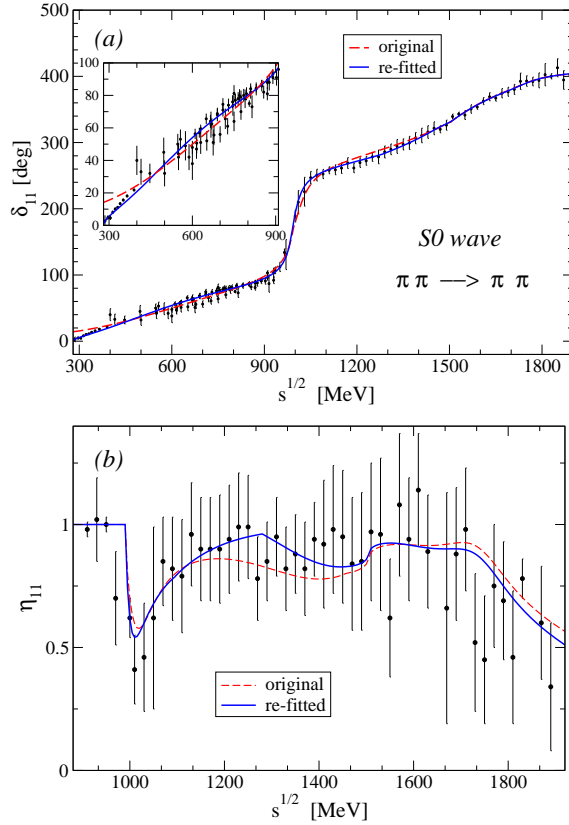


FIG. 4: Results of the original $S0$ (dashed line) and re-fitted (after fitting to data and dispersion relations) $S0$ (solid line) amplitudes for the phase shift (a) and inelasticity (b) of the $\pi\pi \rightarrow \pi\pi$ scattering are compared with experimental data.

can be also seen from a comparison of the initial and re-fitted values of the χ^2_{Data} in Table VI. Such comparison

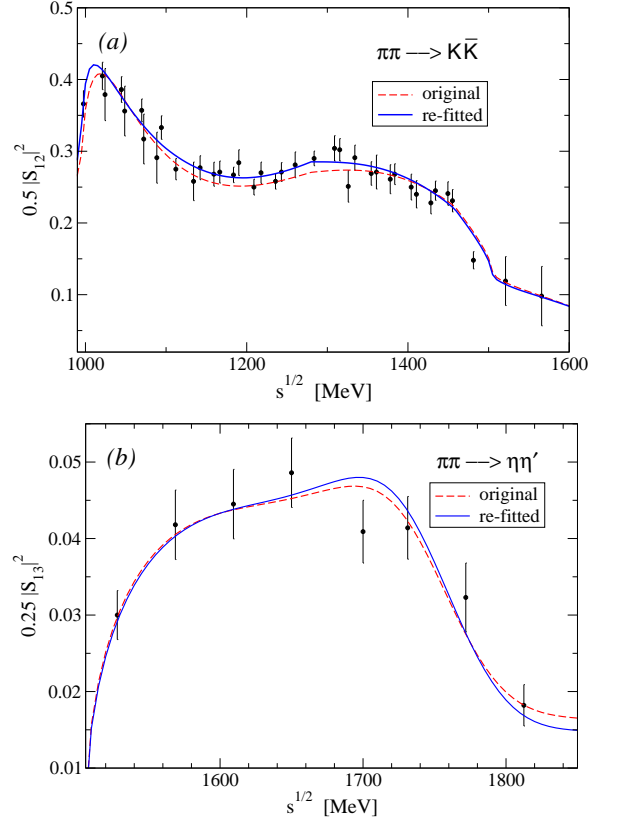


FIG. 5: The same as in Fig. 4 for the squared modulus of the S matrix for the $\pi\pi \rightarrow K\bar{K}$ (a) and $\pi\pi \rightarrow \eta\eta'$ (b).

is more complicated for the $D0$ amplitude since there are more resonance states with more free parameters. Analysis shows that some $D0$ resonances are irrelevant and some of them have weighty decay widths (f_{ri}) only in two or three channels. For example, the decay widths of $f_2(1640)$ into the $\pi\pi$ and $\eta\eta$ channels are practically zero after the dispersive analysis (compare Tables I and XIII) which is compatible with PDG [14] where only the $2\pi 2\pi$ and $K\bar{K}$ decays are seen. Similarly the $f_2(2300)$ resonance reveals a very weak coupling/branching to the $2\pi 2\pi$ channel after the dispersive analysis. The $f_2(1525)$ resonance with a negligible decay width into the $\pi\pi$ channel [14] has also a small value of the parameter f_{r1} in our analysis. Note that in the latest issue of PDG [14] only decays of the $f_2(1270)$ and $f_2(1525)$ resonances into the $\pi\pi$, $2\pi 2\pi$, $K\bar{K}$, and $\eta\eta$ channels are precisely determined whereas for the other resonance states mostly a status “seen” is reported.

Results for the phase shifts and inelasticities for the $D0$ and $F1$ waves are presented in Figs. 1 - 3. The dispersive analysis practically did not affect the description of the elastic phase shifts δ_{11} in both waves. The same holds true for the inelasticity parameter in the $F1$ wave. On the contrary inelasticity in the $D0$ wave for the $\pi\pi \rightarrow \pi\pi$ channel has improved significantly, especially around 1 and 1.3 GeV. In the 1 GeV region the New $D0$ ampli-

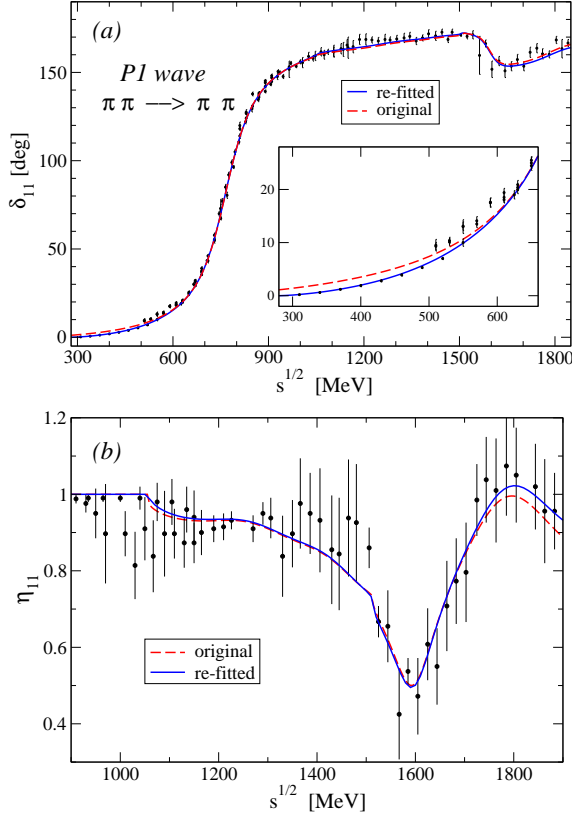


FIG. 6: Results of the original $P1$ (dashed line) and re-fitted (after fitting to data and dispersion relations) $S0$ (solid line) amplitudes for the phase shift (a) and inelasticity (b) of the $\pi\pi \rightarrow \pi\pi$ scattering are compared with experimental data and pseudo data points.

state	M_r	f_{r1}	f_{r2}	f_{r3}	f_{r4}
$f_2(1270)$	1275.5	451.6	77.3	121.0	64.7
$f_2(1525)$	1570.7	76.3	400.8	999.0	922.9
$f_2(1640)$	1639.0	0.002	356.3	222.0	0.0002
$f_2(1810)$	1815.0	120.4	813.0	999.0	873.2
$f_2(2150)$	2157.0	11.7	842.8	803.4	999.0
$f_2(2300)$	2181.6	27.0	0.0005	453.5	142.9

TABLE XIII: Parameters of the Breit-Wigner form (in MeV) for the $D0$ wave after fitting in the SPDF analysis. The initial values of the parameters are in Table I. The masses were not changed in the dispersive analysis.

tude slightly violates unitarity which has been cured in its re-fitted version. The description becomes slightly worse around 1.5 GeV. One can also say that the modulus squared of S_{13} ($\pi\pi \rightarrow K\bar{K}$) is also more realistic after the dispersive analysis, especially in the peak region. Noticeable changes are also apparent in behavior of $|S_{14}|^2$ ($\pi\pi \rightarrow \eta\eta$) in Fig. 2(b).

We have performed various fits to learn which $D0$ resonance states are dominant or ineffective in our approach. Results show that not all first four lightest states, i.e.

state	M_r	f_{r1}	f_{r2}	f_{r3}	f_{r4}
$\rho_3(1690)$	1713.7	291.6	497.8	0.0	0.0

TABLE XIV: Parameters of the Breit-Wigner form (in MeV) for the $F1$ wave after fitting in the SPDF analysis. The initial values of the parameters are in Table II. The mass of the resonance was not changed in the dispersive analysis.

$f_2(1270)$, $f_2(1430)$, $f_2(1525)$, and $f_2(1640)$, are the most relevant states in the analysis, as one would naively expect. This is demonstrated in Table XV which shows the χ^2 for the fits with one particular resonance omitted.

The χ^2 was composed of the χ^2_{Data} for the $D0$ wave and χ^2_{DR} for all partial-waves. Values of the χ^2 in the fits No. 9, 11, and 12 are almost equal to the value in the fit No. 1 with all resonance states included. Accordingly, one can conclude that the $f_2(2010)$, $f_2(2300)$, and $f_2(2340)$ resonances are insignificant in the description. Values of the χ^2 in the fits No. 3, 5, 7, and 8 show that although the $f_2(1430)$, $f_2(1640)$, $f_2(1910)$ and $f_2(1950)$ do not play a very important role in the data description one should keep them. The other states, $f_2(1525)$, $f_2(1810)$, and $f_2(2150)$, influence behavior of the amplitude even more. Obviously the most significant resonance which dominates behavior of the amplitude is the $f_2(1270)$ resonance.

Fit No.		$\chi^2/n.d.f.$
1	All states included	326.21/330=0.9885
Omitted Resonances		
2	$f_2(1270)$	5838.8/330=17.69
3	$f_2(1430)$	327.39/330=0.9921
4	$f_2(1525)$	336.97/330=1.0211
5	$f_2(1640)$	327.76/330=0.9932
6	$f_2(1810)$	348.07/330=1.0548
7	$f_2(1910)$	327.36/330=0.9920
8	$f_2(1950)$	327.26/330=0.9917
9	$f_2(2010)$	326.68/330=0.9899
10	$f_2(2150)$	368.81/330=1.1176
11	$f_2(2300)$	326.54/330=0.9895
12	$f_2(2340)$	326.64/330=0.9898

TABLE XV: Values of χ^2 after fitting with omitted some specific resonance state in the $D0$ wave.

A. Full $\pi\pi$ amplitude

The set of all important partial-wave amplitudes modified and re-fitted in the previous sections allowed us to construct the full $\pi\pi$ amplitude and to calculate the total and differential $\pi\pi \rightarrow \pi\pi$ cross section up to about 2 GeV. In the following we briefly summarize the basic formulas to clarify the normalization and the partial-

wave decomposition.

The partial-wave amplitudes are related to the phase shift and inelasticity as

$$t_\ell^I(s) = \frac{\sqrt{s}}{4ik_1} [\eta_\ell^I(s) e^{2i\delta_\ell^I(s)} - 1] \quad (10)$$

and summed with the Legendre polynomials $P_\ell(\cos\theta)$ give the full invariant $\pi\pi$ amplitude $\mathcal{T}^I(s, t)$ in a given isospin channel I

$$\mathcal{T}^I(s, t) = 32\pi \sum_\ell (2\ell + 1) t_\ell^I(s) P_\ell(\cos\theta), \quad (11)$$

where θ is the scattering angle between two pions in the c.m. frame.

The full invariant amplitude for the $\pi^+\pi^-$ scattering is

$$\mathcal{T}_{\pi^+\pi^-}(s, t) = \frac{1}{3} \mathcal{T}^0(s, t) + \frac{1}{2} \mathcal{T}^1(s, t) + \frac{1}{6} \mathcal{T}^2(s, t) \quad (12)$$

which gives the differential cross section in the c.m. frame

$$\frac{d\sigma_{\pi^+\pi^-}}{d\Omega} = \frac{1}{64\pi^2 s} |\mathcal{T}_{\pi^+\pi^-}|^2, \quad (13)$$

and the total cross section

$$\sigma_{\pi^+\pi^-}^{tot}(s) = \frac{\text{Im}\mathcal{T}_{\pi^+\pi^-}(s, \theta=0)}{2k_1\sqrt{s}}. \quad (14)$$

The total cross section and its components from the individual partial-waves are presented on Fig. 7. Well seen is the dominance of the $f_0(500)$ and $\rho(770)$ below 1 GeV. Two maxima above this energy are formed mostly by $f_2(1270)$ and $\rho_3(1690)$. Other waves - S_2 and D_2 have minor influence on the cross section. Our theoretical predictions very well agree with data from [12, 18]. Worthy is to notice that such good agreement has been achieved without fitting directly to these data. Uncertainties of the total cross sections presented on the figure were calculated using the Monte Carlo method for 1000 randomly generated sets of all free, in minimizations, parameters taken within their 1σ deviation.

In many experimental analyses performed in the seventies (see some papers in [12, 19]) the $f_0(500)$ was replaced by a very broad and heavier (with mass around 1 GeV) resonance. Its influence on the phase shifts and cross sections was weaker and distributed in a wider energy range. Therefore, it is interesting to see how the cross section would look if the $f_0(500)$ has been removed from the analysis. We demonstrate it on Fig. 8. Of course the main difference, in comparison with Fig. 7, concerns region below 0.7 GeV which is almost completely determined by the $f_0(500)$. Small enhancement near the $\pi\pi$ threshold is caused by the fixed scalar-isoscalar scattering length and the slope parameter. It is worth to pay attention on completely different behavior of the cross section on Figs. 7 and 8 near the $K\bar{K}$ threshold where one observes the $f_0(980)$. In the cross sections without

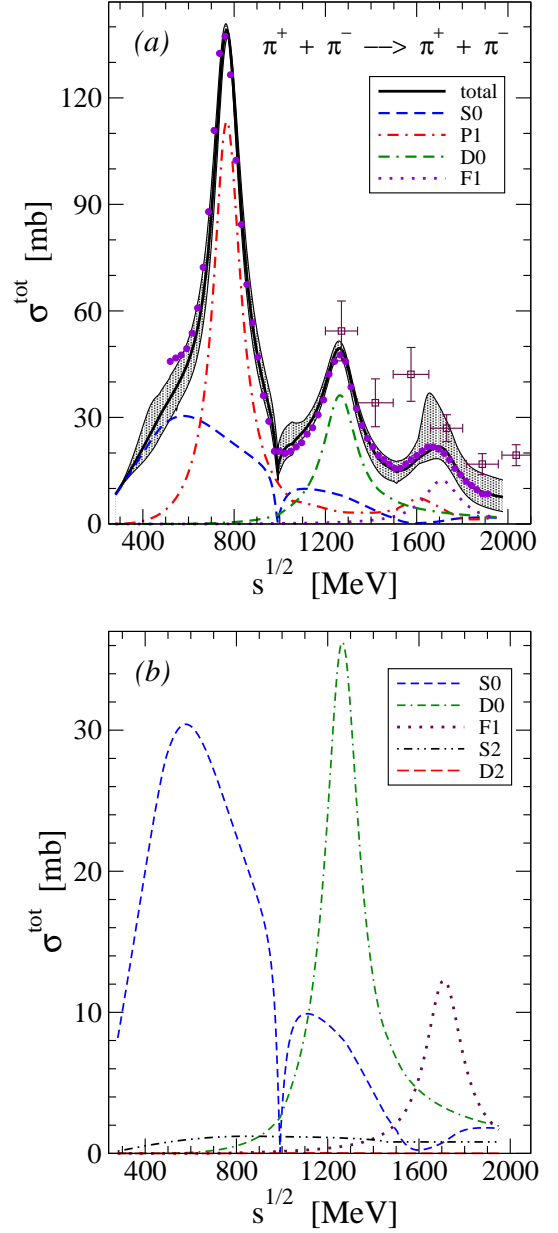


FIG. 7: Prediction of the total cross section in the low-energy region is shown for the $\pi^+\pi^- \rightarrow \pi^+\pi^-$ scattering. Presented are the contributions from most important partial-waves (a) and also for weaker amplitudes (b). The gray band on (a) represents uncertainties of the total cross section. Data are from [12] (dots) and [18] (the six points above 1200 MeV with bigger errors).

the $f_0(500)$ clearly seen is a small peak instead of the deep minimum seen on Fig. 7. The peak appears due to absence of about 90 degree component in the S wave phase shift generated by the $f_0(500)$ pole and zero. On Fig. 8 one can also see that the interference of the $f_0(500)$ with all other amplitudes is positive in the whole energy range except of the region between around 1.5 GeV and 1.7 GeV and vicinity of the small peak around 1 GeV.

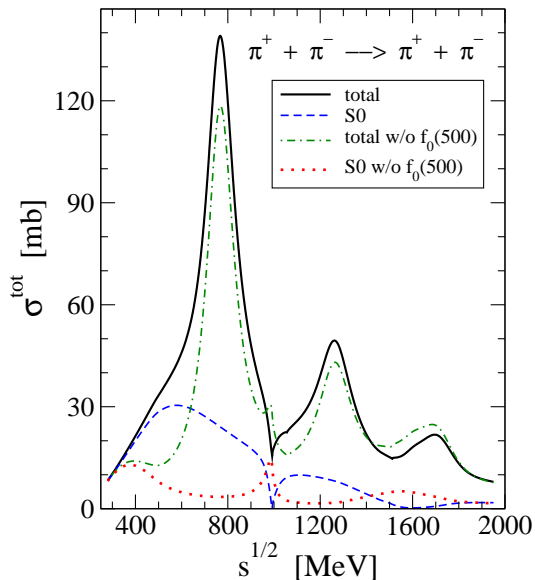


FIG. 8: Prediction of the total and S -wave cross sections in the low-energy region with and without $f_0(500)$ are shown for the $\pi^+ \pi^- \rightarrow \pi^+ \pi^-$ scattering.

The elastic differential cross sections at two energies: 550 MeV and 770 MeV are presented on Fig. 9. Clearly seen is, as expected, the significant role of the S -wave at 550 MeV (dominated by the $f_0(500)$). An interference between the S and P waves producing the enhancement at forward angles is substantial and interference with other waves - only noticeable. In vicinity of the $\rho(770)$ the cross section is, of course, dominated by the P -wave. Again, the interference between the S and P waves is very important and interference with other waves barely noticeable.

VI. CONCLUSIONS

We have constructed new multi-channel $D0$ - and $F1$ -wave $\pi\pi$ amplitudes using the multi-channel Breit-Wigner formalism. When constructing the $D0$ wave we utilized the tensor-isoscalar resonances presented in the latest issue of the PDG tables. We showed that the data in the $F1$ -wave can be satisfactorily described considering only one resonance $\rho_3(1690)$. The other state $\rho_3(1990)$ also listed in PDG appeared as unnecessary in the data description.

The previously constructed $S0$ - and $P1$ -wave multi-channel amplitudes and the new ones, $D0$ and $F1$, were modified in the dispersive analysis using the Roy-like equations (GKPY). The isotensor amplitudes $S2$ and $D2$, also used in the analysis, were taken in the phenomenological form and were not changed.

The modified (re-fitted) partial-wave multi-channel amplitudes $S0$, $P1$, $D0$, and $F1$ are optimized to the experimental data in the considered channels and they

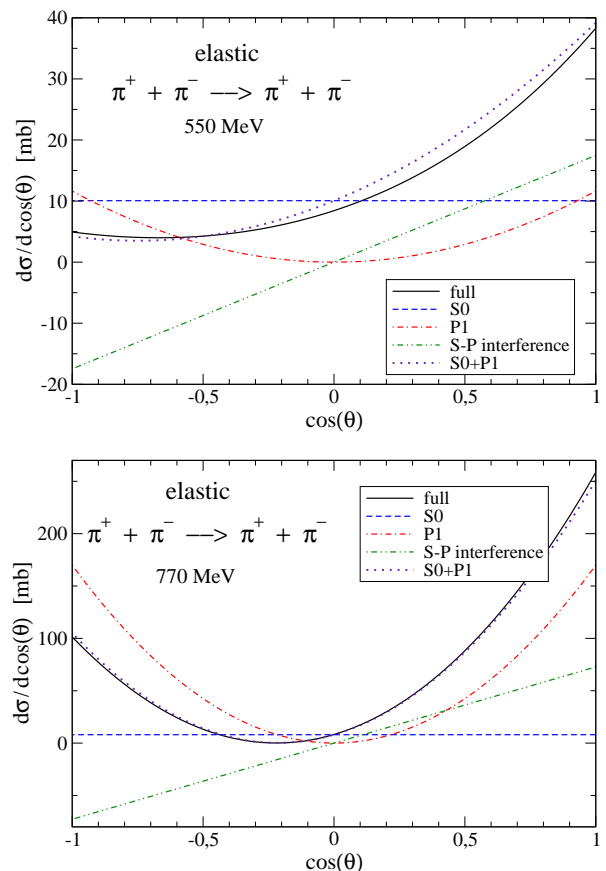


FIG. 9: Angular dependence of the cross section for two energies is shown as predicted in the $\pi^+ \pi^-$ scattering. Contributions from particular partial-waves are shown.

fulfill the crossing symmetry condition imposed by the GKPY dispersion equations. The overall description of the data is satisfactory. In the $S0$ -wave amplitude a position of the $f_0(500)$ pole on the second Riemann sheet was changed to the value very well consistent with the PDG values and with our previous result. In the analysis of the $D0$ wave we concluded that apart of the dominant $f_2(1270)$ state the resonances $f_2(1525)$, $f_2(1810)$, and $f_2(2150)$ also do play an important role in the data description and are also required in the dispersive analysis.

The modified partial-wave amplitudes were utilized in constructing the full invariant $\pi\pi$ scattering amplitude and the cross sections were calculated.

ACKNOWLEDGEMENT

We want to thank Yurii S. Surovtsev for his help and many useful discussions with him. We are particularly grateful to George Rupp for many important comments and observations, and for very fruitful discussions with one of us. This work has been partially supported by the Polish Science Center (NCN) Grants No. Dec-

2013/09/B/ST2/04382 and DEC-2014/15/N/ST2/03504 and by the Grant Agency of the Czech Republic under

the grant No. P203/15/04301.

-
- [1] B. Ananthanarayan, G. Colangelo, J. Gasser and H. Leutwyler, Phys. Rept. **353**, 207 (2001).
 - [2] R. Garcia-Martin, R. Kamiński, J.R. Pela'ez, J. Ruiz de Elvira and F.J. Yndurain, Phys. Rev. D **83**, 074004 (2011).
 - [3] J. R. Pela'ez and F. J. Yndurain, Phys. Rev. D **71**, 074016 (2005).
 - [4] R. Kamiński, Int. J. Mod. Phys. Conf. Ser. **39**, 1560087 (2015).
 - [5] K. Nakamura *et al.* (Particle Data Group), J. Phys. G **37**, 075021 (2010).
 - [6] "2013 Review of Particle Physics" J. Beringer *et al.* (Particle Data Group), Phys. Rev. D **86**, 010001 (2012).
 - [7] S. M. Roy, Phys. Lett. B **36**, 353 (1971).
 - [8] P. Bydžovský, R. Kamiński, V. Nazari, Phys. Rev. D **90**, 116005 (2014).
 - [9] Yu. S. Surovtsev, P. Bydžovský, R. Kamiński and M. Nagy, Phys. Rev D **81**, 016001 (2010).
 - [10] Yu. S. Surovtsev, P. Bydžovský, R. Kamiński and M. Nagy, arXiv:1104.0538 [hep-ph].
 - [11] R. Kaminski, Phys. Rev. D **83**, 076008 (2011).
 - [12] B. Hyams *et al.*, Nucl. Phys. B **64**, 134 (1973).
 - [13] S.J. Lindenbaum and R.S. Longacre, Phys. Lett. B **274**, 492 (1992); R.S. Longacre *et al.*, Phys. Lett. B **177**, 223 (1986).
 - [14] K. A. Olive *et al.* (Part. Data Group) Chin. Phys. C **38**, 090001 (2014).
 - [15] I. Caprini, G. Colangelo, H. Leutwyler, Phys. Rev. Lett. **96**, 132001 (2006).
 - [16] R. Garcia-Martin, R. Kamiński, J.R. Pela'ez and J. Ruiz de Elvira, Phys. Rev. Lett. **107**, 072001 (2011).
 - [17] V. Nazari, R. Kamiński, Acta Phys. Polon. B **46**, 1355 (2015).
 - [18] N.N. Biswas *et al.*, Phys. Rev. Lett. **18**, 273 (1967).
 - [19] P. Estabrooks and A. D. Martin, Nucl. Phys. B **79**, 301 (1974); S. D. Protopopescu *et al.*, Phys. Rev. D **7**, 1279 (1973); R. Kamiński, L. Leśniak, and K. Rybicki, Z. Phys. C **74**, 79 (1997); Eur. Phys. J. direct C **4**, 1 (2002); B. Hyams *et al.*, Nucl. Phys. B **100**, 205 (1975); M. J. Losty *et al.*, Nucl. Phys. B **69**, 185 (1974); W. Hoogland *et al.*, Nucl. Phys. B **126**, 109 (1977); N. B. Durusoy *et al.*, Phys. Lett. **45B**, 517 (1973); G. Grayer *et al.*, Nucl. Phys. B **75**, 189 (1974).